ELSEVIER

Chemical Engineering Journal 137 (2008) 244–250

Chemical Engineering Journal

www.elsevier.com/locate/cej

Isothermal adsorption equilibrium and dynamics of binary mixture gasoline constituents on honeycomb monoliths

Dae Jung Kim [a], Namgoo Kang [b,*], Wang Geun Shim [c], Seoung Hyun Kim [d]

[a] *Department of Chemistry and Biochemistry, Texas Tech University, Lubbock, TX 79409-1061, United States*
[b] *Division of Metrology for Quality Life, Korea Research Institute of Standards and Science, Daejeon 305-340, South Korea*
[c] *Faculty of Applied Chemistry, Chonnam National University, Kwangju 500-757, South Korea*
[d] *Department of Environmental Engineering and Biotechnology, Myongji University, Yongin 449-728, South Korea*

Received 11 October 2006; received in revised form 12 April 2007; accepted 22 April 2007

Abstract

Investigations of multiple-component isothermal adsorption dynamics are indispensable to a better understanding of the performance of automobile exhaust gas cleaning systems particularly in the stage of cold start. Dual-component adsorption isotherm equilibrium and dynamics at 323.15 K were explored experimentally in this study. A ZSM5-coated (Si/Al = 150) monolithic hydrocarbon absorber (ADS #1) and a monolithic light-off catalyst (CAT #1) were used as the model adsorbents. 2,2,4-Trimethylpentane (TMP) and toluene were chosen as the model gasoline constituents. In the dual-component system of TMP and toluene, TMP emitted earlier than toluene under the typical conditions where both are relatively comparable in the molar fractions in the gas phase. However, the reversed breakthrough occurred under the conditions where toluene was predominant over TMP in the molar fraction in the gas phase.

Keywords: ZSM5; Adsorption equilibrium; Langmuir–Freundlich isotherm; Gasoline; Toluene; 2,2,4-Trimethylpentane

1. Introduction

Recently stringent regulations for the emissions of a vehicle cannot be met easily with conventional three-way catalysts under certain conditions. These catalysts are usually inactive during cold start of an engine, as they require a temperature level of at least around 300 °C for adequate performance. Therefore, most hydrocarbon emissions for a typical vehicle occur mainly in the stage of cold start. To meet the emission regulations, the quantity of incompletely converted hydrocarbons must be reduced. Emission reduction technologies such as close-coupled catalyst [1] and hydrocarbon adsorbers [2] have been developed. A hydrocarbon adsorber system is typically composed of a hydrocarbon adsorber and a light-off catalyst. The absorber is capable of capturing hydrocarbons on zeolite or other adsorbent materials during cold start. As the absorbent become heated up, the adsorbed hydrocarbons start to desorb and then convert into carbon dioxide and water by the heated light-off catalyst in the presence of molecular oxygen. Once the light-off catalyst is heated up enough to allow the conversion of the hydrocarbons, the liberation of the hydrocarbons to the ambient air diminishes.

A number of studies have been documented primarily on engines and vehicle experiments [3]. It is yet difficult to obtain thermodynamic information involving adsorption equilibria within a range of temperature during the span of cold start. Components of hydrocarbons generated from an engine during cold start are dependent greatly on the type of fuel and the performance of the engine as well as start-up conditions. Whatever the conditions, the emissions of 2,2,4-trimethylpentane (TMP) and toluene in considerable quantities have been reported [4].

The earlier publications provided experimentally major characteristics of the single-component adsorption isotherms for TMP and toluene [5–7]. Others reported the fundamental characteristics of ZSM5-coated monoliths [8] and single-component adsorption of selected hydrocarbons for selected hydrocarbons [9]. The information on the adsorption equilibrium and dynamics of hydrocarbons in binary mixture is currently unavailable. It is imperative that adsorption phenomena at the stage of cold start needs to be furthered especially concerning adsorbate mixtures. To this end, dynamic adsorption behavior of the two model

* Corresponding author. Tel.: +82 42 868 5221; fax: +82 42 868 5042.
E-mail address: nkang@kriss.re.kr (N. Kang).

1385-8947/$ – see front matter © 2007 Elsevier B.V. All rights reserved.
doi:10.1016/j.cej.2007.04.026

adsorbates in binary mixture on ZSM5-coated monolithic adsorber systems were explored in this study. ZSM5, in which the ratio of Si and Al was 150, was employed in this work because of its better resistance against moisture and enhanced thermal stability relative to 100% Si-based absorbate. In addition to the presentation of experimental results, a set of mathematical adsorption models to describe both equilibrium and dynamics of the investigated systems are proposed in this research. In addition, the effect of molecular oxygen on hydrocarbon adsorption on the test adsorbent was also experimentally tested.

2. Experimental

2.1. Preparation of adsorbents and adsorbates

ZSM5-coated cordierite monoliths (Fig. 1), hydrocarbon adsorber and light-off catalyst, used in this study were denoted as ADS #1 and CAT #1, respectively. The procedures to prepare ADS #1 and CAT #1 are summarized herein, and refer to elsewhere for details [5–7,10]. ADS #1 was prepared by coating the washcoat onto honeycomb ceramic substrates. The washcoat consisted of γ-Al_2O_3 (80%), ZSM5 zeolite (20%) with a Si/Al ratio of 150/1, and base metals (Ba, Ce, and Zr). Al-ZSM5 was employed due to its higher resisting performance against moisture (i.e., thermal stability) than that of H-ZSM5 (100% Si). The absorber was impregnated with precious metals (Pd/Rh = 10/1) by adding solutions of $PdCl_2$ and $RhCl_3{\cdot}3H_2O$ to the slurry of the washcoat. After metal impregnation, the substrate was dried at 150 °C for 5 h and calcined at 600 °C for 4 h. The loading amounts of the washcoat and precious metals were 140 and 4.5 g/L, respectively. CAT #1 was prepared in the same manner but did not contain ZSM5 zeolite, and the loading amount of precious metals was 3.5 g/L.

The physical properties of the two adsorbents are presented in Table 1. The cell densities of the substrates were 62 cells/cm^2. The dimension of the samples was 1.9 cm in diameter and 3 cm in length. The wall thickness of the substrates and the washcoat thickness of the adsorbers were measured by a SEM (Phillip 505) with an EDS detector. Surface and pore volumes were determined by an N_2 volumetric adsorption apparatus (AS1, Quantachrom).

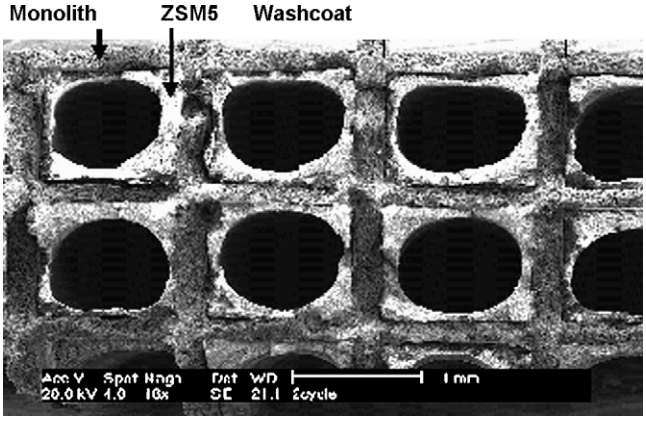

Fig. 1. A cross-sectional view of ZSM5-coated cordierite monolith.

Table 1
Physical properties for the two adsorbents used

Adsorbent	ADS #1	CAT #1
Geometric surface area per unit volume of monolith (m^2/m^3)	2634	2639
Hydraulic diameter (mm)	1.062	1.064
Channel wall thickness (mm)	0.208	0.206
Channel wall density (kg/m^3)	2988	2993
BET surface area (m^2/g)	74	49
Void fraction of the channel wall	0.28	0.29
Overall void fraction	0.76	0.77

TMP (Aldrich, 99.8%) and toluene (Aldrich, 99.95%) were used as the model adsorbates without any further treatment. To probe the impact of molecular oxygen on adsorption behavior, oxygen gas of ultra high-purity (99.999%) grade was used.

2.2. Adsorption experiments

Isothermal dynamic adsorption experiments were conducted using the apparatus presented in the previous papers [6,7,11]. Prior to each experiment, the adsorbent samples were exposed to air at a flow rate of 1 L/min and 673.15 K for 1 h and purged using N_2 at 1 L/min and 673.15 K for 1 h and then cooled down to 303.15 K under N_2 at 1 L/min. After that, single or two hydrocarbons at a total of 1000 ppm (0.1 kPa) under N_2 at 0.5–2 L/min was continuously supplied to each adsorbent at 323.15 K until the end of each adsorption experiment.

2.3. Analytical methods

The concentrations of hydrocarbons at the entrance and the exit of the reactor were monitored using FTIR (Nicolet) with a mercury–calcium–telluride detector, which was cooled by liquid N_2 in a gas cell, and with 16 scans and a resolution of 2 cm^{-1}. The concentrations were also re-monitored by a gas chromatograph (Hewlett-Packard HP5890 Plus) equipped with a flame ionization detector and a capillary column (DB1). The vapor pressures of the hydrocarbons were calculated by using the Reid equation [11].

3. Numerical simulation

The proposed model considered a single cellular channel of monolith adsorbent geometry, assuming a steady-state flow with no axial dispersion. In monolith applications, the Peclet number (*Pe*) is typically used.

$$Pe = \frac{uL}{D_L} \tag{1}$$

where u is interstitial velocity (m/s), L is the length of a monolith channel (m), D_L is axial dispersion coefficient (m/s). For automobile applications, its values fall typically within 2000–8000

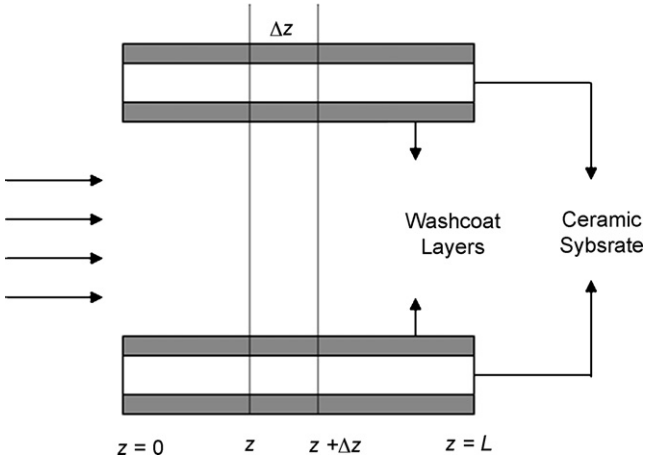

Fig. 2. Schematic diagram of a single cellular channel used in the proposed model.

[12], which validates the assumption of no axial dispersion. The model system was constructed based on the presence of two phases: the adsorbates in the vapor phase and the channel wall having washcoat and ceramic substrate layers in the solid phase. A schematic diagram of a single cellular channel is shown in Fig. 2.

In this study, the adsorption equilibrium relationships were represented by an extended Langmuir–Freundlich (ELF) isotherm because of its simplicity due to the explicit formula and the reasonable prediction accuracy validated by some volumetric adsorption experiments [13,14]. The mass transfer rate on the surface of the channel wall was approximated by a linear driving force expression [15]. This expression holds an assumption that mass transfer rate of adsorption is proportional to the difference between the equilibrium concentration and the bulk concentration of an adsorbate. The entire assumptions made in developing an isothermal dynamic adsorption model are summarized as follows:

1. The ideal gas law applies.
2. The system is a multiple-component adsorption system under an isothermal condition.
3. The gas velocity is constant in the cellular channel.
4. The pressure gradient and axial dispersion across the cellular channel are negligible.
5. Radial temperature, concentrations, and velocity gradients within the channel are negligible.
6. The mass transfer rate is represented by a linear driving force expression.
7. The multi-component adsorption equilibrium is represented by the extended L–F isotherm equation.
8. There are no reactions on the surface of the channel wall.
9. Adsorption occurs only on the channel wall.

After applying the aforementioned assumptions for the components and total mass balances in the gas phase, the following set of equations is formulated to describe an isothermal adsorption system.

Mass balance for component i in the gas phase is

$$\frac{\partial y_i}{\partial t} = -u\frac{\partial y_i}{\partial z} - \frac{1-\varepsilon_p}{\varepsilon_p}\rho_{cw}\frac{\partial \bar{q}_i}{\partial t}\frac{1}{C_T} \tag{2}$$

where y_i is the molar fraction of component i in the gas phase, t is the elapsed time, z is the axial distance coordinate (m), ε_p is the overall void fraction, ρ_{cw} is the density of the channel wall (kg/m^3), $\bar{q}_i$ is the adsorbed amount of component i in the solid phase (mol/kg), and C_T is the total concentration (mol/m^3).

Mass balance for component i in the solid phase is

$$\rho_{cw}\frac{\partial \bar{q}_i}{\partial t} = a_M k_M C_T(y_i - y_{i,s}) \tag{3}$$

where a_M is the geometric surface area per unit volume of the monolith (m^2/m^3), k_M is the mass transfer coefficient (m/s), and $y_{i,s}$ is the molar fraction of component i in the solid phase.

Initial conditions for $0<z<L$ and $t=0$ are

$$y_i = 0, \qquad \bar{q}_i = 0 \tag{4}$$

Boundary condition for $z=0$ and $t>0$ is

$$y_i = y_{i0} \tag{5}$$

The ELF adsorption isotherm for a multi-component system is

$$\bar{q}_i = \frac{q_{mi}b_i(Py_{i,s})^{ni}}{1+\sum_{j=1}^{n} b_j(Py_{j,s})^{nj}} \tag{6}$$

where q_m is the adsorbed amount of component i in the solid phase (mol/kg), b is the absorption isotherm parameter, and P is total pressure (kPa). Subscript i refers to each hydrocarbon under consideration (e.g., TMP and toluene for the dual-component adsorption system in this study). The isotherm parameters of TMP and toluene on the adsorbents are listed in Table 2. The mass transfer coefficient of a component in the channels of a monolith, k_M, under a laminar flow can be estimated by empirical or theoretical methods. Among a variety of methods, a correlation model proposed by Hawthorn [16] was employed in this study because the relationship originated from monolithic light-off catalytic reactors under the conditions typically occurring in automobile exhaust gas cleaning systems.

$$Sh = \frac{k_M d_{ch}}{D_e} = 2.976\left(1 + 0.095 ReSc\frac{d_{ch}}{L}\right)^{0.45} \tag{7}$$

$$Re = \frac{\rho u d_{ch}}{\mu}, \qquad Sc = \frac{\mu}{\rho D_e} \tag{8}$$

where Sh, Re, and Sc are the Sherwood, the Reynolds, and the Schmidt numbers, respectively. d_{ch} is the hydraulic diameter inside the channel (m), D_e is the effective diffusivity (m^2/s), ρ is the gas density (kg/m^3), and μ is the gas viscosity (kg/m s).

In Eq. (8), the effective diffusivity of a species inside the channel, D_e, was estimated by the following equation that considered pore diffusion [13].

$$D_e = \frac{\varepsilon_{cw}}{\tau}97 d_p\left(\frac{T}{M_w}\right)^{0.5} \tag{9}$$

Table 2
Langmuir–Freundlich isotherm parameters of each single-component adsorption system for 2,2,4-trimethylpentane (TMP) and toluene

Adsorbent	TMP			Toluene		
	q_m (mol/kg)	b (kPa^{-1})	n	q_m (mol/kg)	b (kPa^{-1})	n
ADS #1	1.179	0.074	0.225	1.053	0.213	0.242
CAT #1	0.552	0.229	0.581	1.691	0.097	0.353

where ε_{cw} is the void fraction of the channel wall, τ is the tortuosity factor, d_p is the mean pore diameter (m), T is the adsorption temperature (K), and M_w is the molecular weight of a species (g/mol).

Hayes et al. [17] reported that the tortuosity factor of about 8.0 was appropriate for the monolith catalysts with washcoat layers. Thus, this value was employed in the present study for both adsorbents. The mean pore diameters were 15 and 18 nm for ADS #1 and CAT #1, respectively. The values of the constants used in the model are listed in Table 2.

To seek the numerical solutions to the proposed model equations, an orthogonal collation method was utilized [18]. The numerical solution sets were integrated by the DVODE solver [19].

4. Results and discussion

4.1. Single-component adsorption

The breakthrough curves of TMP and toluene on ADS #1 at 323.15 K are shown in Fig. 3. The inlet concentrations of the two adsorbates were identical as 1000 ppm (0.1 kPa) and the other conditions including the average gas velocity (u = 7.56 cm/s) and sample length (L = 3 cm) were also equal. TMP was emitted earlier than toluene under identical isothermal conditions. These results may be due to the significant difference in adsorption affinity on the adsorbent.

The breakthrough curves of TMP and toluene on CAT #1 at 323.15 K are given in Fig. 4. The experimental conditions used in Fig. 4 were exactly identical to those applied in Fig. 3. The breakthrough order of the two adsorbates was the same as that observed in Fig. 3, implying that toluene has a greater adsorption affinity for the adsorbents than TMP. The adsorption process is a function of microporosities. A comparison of Figs. 2 and 3 exhibits that for the same adsorbate, ADS #1 owned the relatively higher specific surface area and lower pore diameter than CAT #1 (Table 1) due to the amendment of ZSM5 zeolite retaining a mean pore size of 0.6 nm.

The impacts of molecular oxygen on the breakthrough curves for TMP and toluene on ADS #1 were experimentally tested. As the results are demonstrated in Fig. 5, the curves were little affected by the presence of molecular oxygen at its concentration of 1.8 vol% frequently occurring in the exhaust emission gas mixtures. This result indicates that molecular oxygen at 1.8 vol% barely competes for adsorption with TMP at 0.1 kPa, suggesting that adsorption affinity of the hydrocarbon to the surface may be much greater than that of molecular oxygen. For CAT #1, similar results were also observed.

4.2. Dual-component adsorption

The adsorption phase diagrams of TMP and toluene on ADS #1 at 323.15 K are shown in Fig. 6. The open symbols indicate the experimental data, whereas the solid lines indicate the predicted results. The experimental data points were extracted directly from those observed in the breakthrough curves. The diagonal line indicates the ideality in a mixture system defined by Raoult's law that the molar fractions of the two adsorbates in the adsorbed

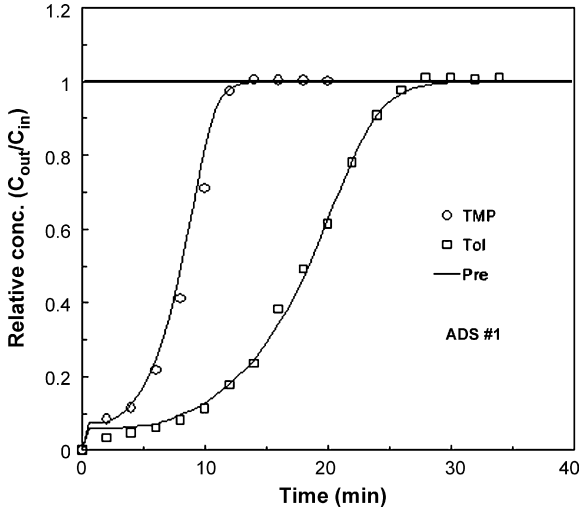

Fig. 3. Single-component breakthrough curves of TMP and toluene on ADS #1 at 323.15 K (L = 3 cm, u = 7.56 cm/s).

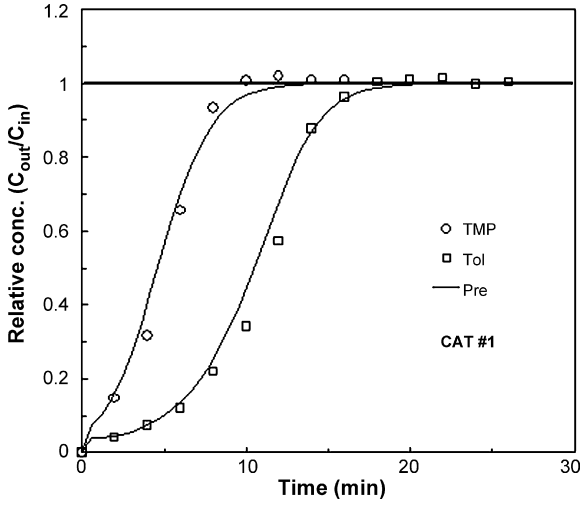

Fig. 4. Single-component breakthrough curves of TMP and toluene on CAT #1 at 323.15 K (L = 3 cm, u = 7.56 cm/s).

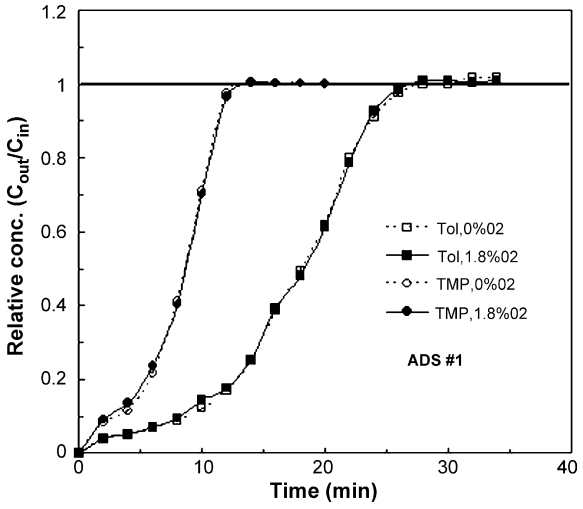

Fig. 5. Single-component breakthrough curves of toluene on ADS #1 at 323.15 K in the absence and the presence of O_2 ($L = 3$ cm, $u = 7.56$ cm/s).

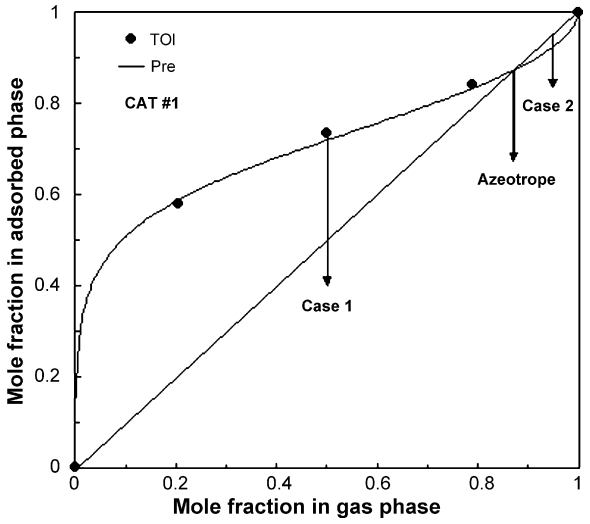

Fig. 7. Adsorbed molar fractions of TMP and toluene in equilibrium on CAT #1 at 323.15 K as a function of molar fraction in the gas phase.

phase are identical to those in the gas phase. Azeotropes occur because of deviations from the Raoult's law. Azeotropes are an indicator in reversed adsorption selectivity [15]. The positive deviations from the Raoult's law were experimentally observed in the region where molar fraction of toluene in the gas phase was between 0 to around 0.76 (azeotrope). On the contrary, the negative deviation from the Raoult's law was found when the molar fraction of toluene vapor was greater than that of azeotrope. The experimental results and the model simulations predicted both positive and negative deviations from the ideality. Overall findings suggest that this adsorbent (ADS #1) is an energetically heterogeneous surface system due to its highly complicated mixture of constituents. As a consequence, the absorbent could cause the nonideal behavior of the adsorbates.

Many have studied nonideal behavior using theoretical models such as real adsorbed solution theory (RAST) and vacancy solution model (VSM) [13,15]. These models were designed to estimate "additional" interaction parameters between two components in order to simulate nonideal behavior in a dual-component adsorption system. Therefore, additional parameter fitting models (e.g., Wilson, UNIQUAC) must be incorporated into the multi-component adsorption model. An advantageous feature of the proposed model is that deviations form the ideality (drawn as diagonal line in Fig. 5) was properly simulated without additional fitting parameter equations that reflect nonideal behavior.

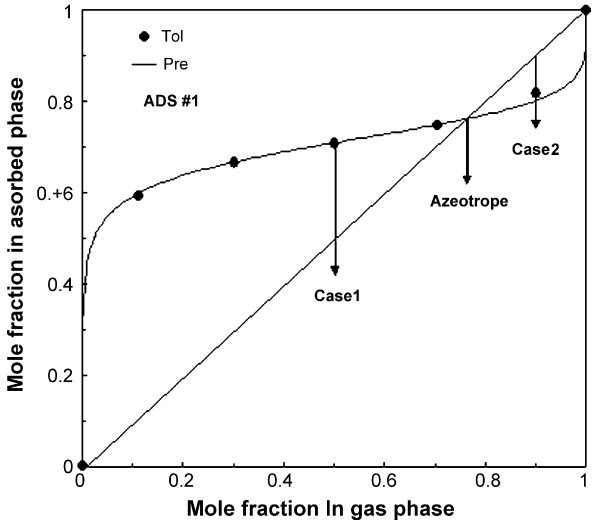

Fig. 6. Adsorbed molar fractions of TMP and toluene in equilibrium on ADS #1 at 323.15 K as a function of molar fraction in the gas phase.

The adsorption phase diagrams of TMP and toluene in equilibrium on CAT #1 at 323.15 K are presented in Fig. 7. With its trend similar to that observed in Fig. 6, the location of the azeotrope point in Fig. 7 shifted toward much higher fraction of toluene in the gas phase (>0.86).

The experimental and the prediction results with respect to dual-component adsorption (TMP and toluene) on ADS #1 under two different cases are exhibited in Fig. 8. In Case 1, the molar fractions of TMP and toluene in the gas phase were identical as 0.5. In Case 2, those values were 0.1 and 0.9 for TMP and toluene, respectively. For both cases, the total concentration of gases was 1000 ppm (0.1 kPa). In Case 1, TMP liberated more rapidly than toluene. In Case 2, however, the breakthrough order of the dual-component emissions was reversed. These findings are consistent with the aforementioned nonideal adsorption behavior potentially involving the surface heterogeneity of the adsorbent as the experimental data point observed in Case 2 from Fig. 6. This surface heterogeneity resulted from a number of different surface constituents of the test adsorbent, ADS #1: the washcoat (loading amount = 140 g/L) of γ-Al_2O_3 and base metals (Ce, Zr, and Ba), the subsequent amendment of ZSM5 zeolite (Si/Al = 150/1), and in turn the impregnation of precious metals (Pd/Rh = 10/1, loading amount = 4.5 g/L as $PdCl_2$ and $RhCl_3{\cdot}3H_2O$).

The experimental and the prediction results of dual-component adsorption on CAT #1 under the conditions identical to those employed in Fig. 8 are displayed in Fig. 9. The total concentration in the gas phase was set to 1000 ppm (0.1 kPa). For

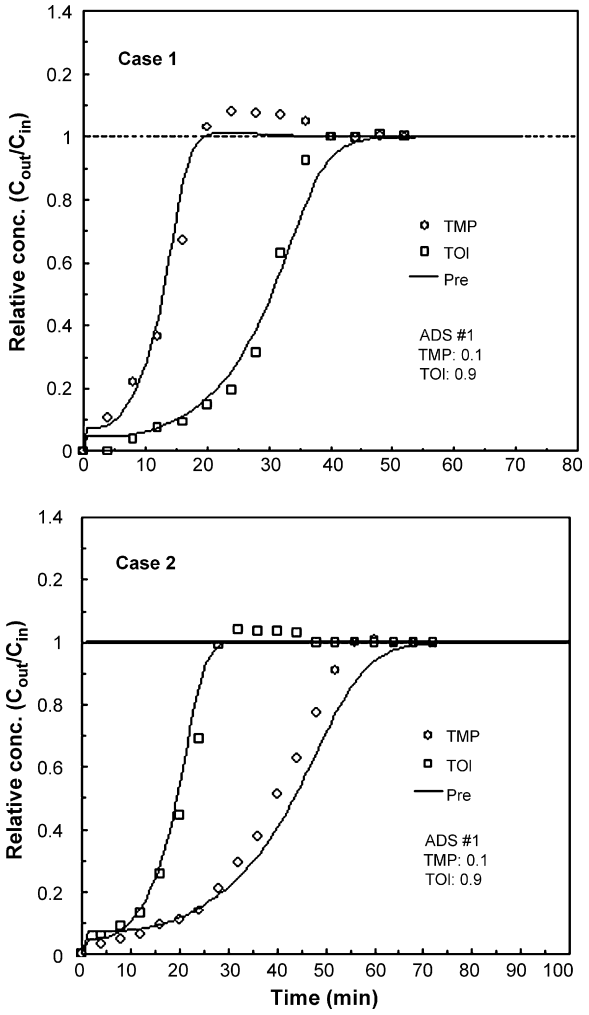

Fig. 8. Dual-component breakthrough curves for TMP and toluene on ADS #1 for Cases 1 and 2 in Fig. 6 ($L = 3$ cm, $u = 7.56$ cm/s).

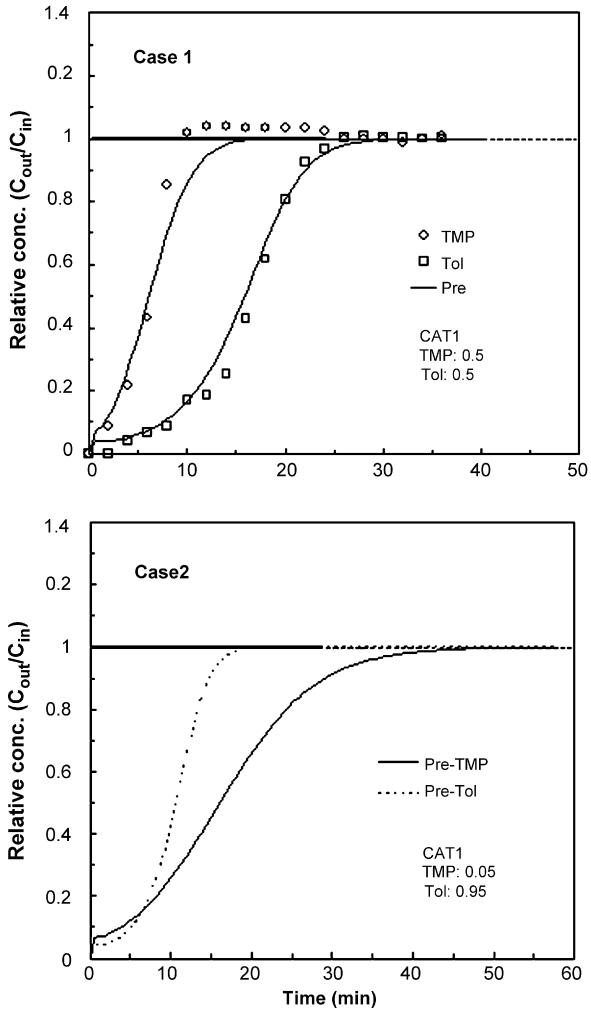

Fig. 9. Dual-component breakthrough curves for TMP and toluene on CAT #1 in Cases 1 and 2 in Fig. 7 ($L = 3$ cm, $u = 7.56$ cm/s).

Case 1 (corresponding to Case 1 in Fig. 7), the molar fractions of TMP and toluene in the gas phase were identical as 0.5. In Case 2 (corresponding to Case 2 in Fig. 7), those values were 0.05 and 0.95 for TMP and toluene, respectively. The observed results were comparable to those observed in Fig. 8. Not surprisingly, the model simulation results indicate that the breakthrough curves of the two components started to cross over each other under the condition where toluene was 19 times greater than that of TMP in molar fraction in the gas phase. As expected, CAT #1 exhibited decreased surface heterogeneity due to the absence of ZSM5 zeolite substrate and a lowered loading amount of 3.5 g/L as compared to the constituents of ADS #1. The proposed surface heterogeneity could cause heterogeneity of adsorption energy, ultimately resulting in the nonideal adsorption behavior of the adsorbates. Comparison of the breakthrough curves on the two adsorbent systems, ADS #1 and CAT #1, shows that the reverse phenomena were much pronounced on ADS #1, suggesting that the impregnation of ZSM5 zeolite into the honeycomb monolith greatly enhanced its surface heterogeneity [6]. The proposed model could predict reasonably the experimentally observed adsorption equilibrium and dynamic behavior in dual-component adsorption systems. In addition, this model predicted nonideal behavior expressed as the occurrence of azeotrope points.

5. Conclusions

Experimental and theoretical studies were conducted in order to evaluate the performance of the two ZSM5-coated adsorbents for the dual-component adsorption of representative volatile gasoline constituents. The experimental results demonstrated that the adsorption affinity of TMP was lower than that of toluene on the ZSM5-coated monoliths of honeycomb shape. For dual-component adsorption systems, however, nonideal behavior was observed under limited conditions where the molar fraction of TMP is much greater than that of toluene in the gas phase. In addition, the breakthrough curves of the hydrocarbons on the adsorbents remained unaffected by the presence of O_2 at 323.15 K. The presented information provides a basis for a better understanding of gas–solid adsorption processes on washcoated monoliths and potential changes to adsorption behavior in a multi-component adsorption system. By potential extension of this dual-component gas–solid adsorption system to a highly complicated multi-component system, the pre-

sented results would be conducive to a design of enhanced automobile exhaust gas cleaning systems. A further study is underway regarding the temperature-gradient adsorption characteristics of binary mixture gasoline compounds on ADS #1 and CAT #1.

References

[1] D.J. Kim, G.S. Son, K.Y. Lee, B.C. Choi, S.R. Kang, J. Korean Soc. Automotive Eng. 4 (1996) 140–146.
[2] J.L. Williams, M.D. Patil, W. Hertl, SAE Paper No. 960343, 1996.
[3] N. Noda, H. Mizuno, J. Suzuki, T. Hiramatsu, P. Busch, SAE Paper No. 1999-01-1230, 1999.
[4] S.Y. Yamamoto, K. Matsushita; S. Etoh, M. Takaya, SAE. Paper No. 2000-01-0892, 2001.
[5] D.J. Kim, J.E. Yie, S.G. Seo, J. Chem. Eng. Data 48 (2003) 1417–1475.
[6] D.J. Kim, J. Colloid Interface Sci. 208 (2004) 290–295.
[7] D.J. Kim, J.M. Kim, J.E. Yie, S.G. Seo, S.-C. Kim, J. Colloid Interface Sci. 274 (2004) 538–542.
[8] Q. Huang, H. Vinh-Thang, A. Malekian, M. Eić, D. Trong-On, S. Kaliaguine, Micropor. Mesopor. Mater. 87 (2006) 224–234.
[9] J. Zamaro, M.A. Ulla, E.E. Miró, Chem. Eng. J. 106 (2005) 25–33.
[10] D.J. Kim, J.W. Kim, J.E. Kim, H. Moon, Ind. Eng. Chem. Res. 41 (2002) 6589–6592.
[11] R.C. Reid, J.M. Prausnitz, B.E. Poling, The Properties of Gases & Liquids, fourth ed., McGraw-Hill, New York, 1988.
[12] K. Umehara, M. Makino, M. Brayer, E.R. Becker, R. Watson, SAE Paper No. 2000-01-0494, 2000.
[13] D.M. Ruthven, Principles of Adsorption and Absorption Processes, Wiley, New York, 1984.
[14] D.J. Kim, G.W. Shim, H. Moon, Korean J. Chem. Eng. 18 (2001) 518–524.
[15] R.T. Yang, Gas Separation by Adsorption Processes, Rutterworths, Boston, 1987.
[16] R.D. Hawthorn, AIChE Symp. Ser. 137 (1974) 428–437.
[17] R.E. Hayes, S.T. Kolaczkowskib, P.K.C. Li, S. Awdry, Appl. Catal. B Environ. 25 (2000) 93–104.
[18] J.V. Villadesen, M.L. Michelsen, Solution of Differential Equation Models by Polynomial Approximation, Prentice-Hall, Englewood Cliffs, NJ, 1978.
[19] P.N. Brown, G.D. Byrne, A.C. Hindmarsh, VODE: a variable coefficient ODE solver, SIAM J. Sci. Stat. Comput. 10 (1989) 1038–1051.